*J. Fluid Mech.* (1967), *vol.* 27, *part* 1, *pp.* 177–207
*Printed in Great Britain*



# Aerodynamics of oscillating disks and a right-circular cylinder

By W. W. WILLMARTH, N. E. HAWK, A. J. GALLOWAY AND F. W. ROOS

Department of Aerospace Engineering, University of Michigan, Ann Arbor

(Received 30 November 1965)

Detailed studies are reported of the free and forced oscillation of disks and a right-circular cylinder constrained to rotate about a fixed diametrical axis passing through the centre of the body and normal to the free-stream direction. When a disk is free to rotate, it oscillates at a definite frequency with slowly varying amplitude and phase. A right-circular cylinder also oscillates at a definite frequency but with rapidly increasing amplitude. When the amplitude becomes large, after a few cycles of oscillation, the cylinder rotates steadily in one direction.

Analogue computer elements, position sensors and a dynamic moment balance were used to study the static restoring moment, dynamic restoring moment, average damping moment, statistical properties of the disk motion and power spectrum of the turbulent moment. The behaviour of the disk and cylinder are explained using the measurements and the theory for random excitation of a linear system. The turbulent exciting moment is caused by the unsteady flow in the wake and can be changed by placing disks and splitter plates in the wake. A model is proposed for the unsteady flow field in the wake behind the disk. The model relates the turbulent moment to the vortex shedding process in the wake.

## 1. Introduction

The flight path and motion of bodies with large regions of separated flow cannot readily be calculated from the equations of motion for the body and fluid. At the present time the only practical way to obtain information about the aerodynamic properties of such bodies is to conduct appropriate experiments. The aerodynamic forces and moments can be calculated from observations of the body motion and flight path, or one can simulate the body motion in flowing fluid and directly measure the pressure distribution or the forces and moments.

We have already studied the motion of freely falling disks (Willmarth, Hawk & Harvey 1963), and observed unsteady motion above a certain critical Reynolds number, between 100 and 170 depending on the moment of inertia of the disk. If the moment of inertia was not too large, translational oscillations of the disk coupled with pitching oscillations about a diameter were observed. When the moment of inertia was large, the disks oscillated with rapidly increasing amplitude and began to tumble. Smith (1953) in a very interesting paper has studied

the motion and aerodynamics of tumbling bodies.† In this paper we describe experimental measurements of the aerodynamic phenomena associated with pitching oscillations of disks and a right-circular cylinder about a fixed axis in a wind tunnel.

We have chosen the disk and right-circular cylinder (hereafter called the cylinder) as extreme examples of bodies with large regions of separated flow and have designed a number of experiments to reveal some of the simplest features of the pitching motion and of the aerodynamic moment acting on the disk and

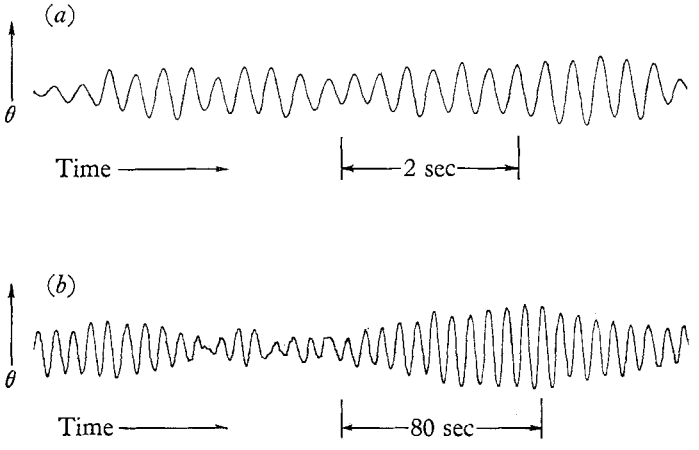


FIGURE 1. Oscillograph records of disk oscillations as a function of time. (*a*) $I^* = 1{\cdot}125$, $nd/U = 0{\cdot}0305$, $d = 12$ in., $h/d = 0{\cdot}104$, $U = 100$ ft./sec, $\sqrt{\overline{\theta^2}} = 0{\cdot}122$ rad. (*b*) $I^* = 42{\cdot}3$, $nd/U = 0{\cdot}0054$, $d = 6$ in., $h/d = 0{\cdot}125$, $U = 100$ ft./sec, $\sqrt{\overline{\theta^2}} = 0{\cdot}041$ rad.

cylinder when they are constrained to rotate about a fixed axis normal to the stream. The separation line on the disk is fixed at the sharp edge when the stream is approximately aligned with the normal to the disk face. The separation line on the cylinder is not as severely constrained and can move over the cylindrical surface from the front to rear face of the cylinder.

When the disk is free to rotate it oscillates at a definite frequency but with varying amplitude and phase. Figure 1 shows representative records of disk oscillations at high and low frequencies. It appears from these records that the amplitude and phase vary slowly enough to allow one to define a definite frequency of oscillation. The disk motion resembles the response of a lightly damped harmonic oscillator to a random forcing function. Oscillations of a cylinder, with length equal to diameter, about a diametrical axis through the centre were also studied. When the cylinder was released from rest with its face normal to the stream, it oscillated a few times with rapidly increasing amplitude and then began to autorotate.

A number of experiments which used an analogue computer for data processing were designed to determine the nature of the aerodynamic driving force for these motions and the nature of the motion itself. The experiments have two purposes: first, to reveal, by studying simple examples, the important aero-

† We are indebted to the reviewer for bringing Smith's paper to our attention.

dynamic features of this and similar problems, and secondly, to develop methods and techniques for use in unsteady aerodynamic problems of this nature.

We shall first outline the linearized theory for the motion about a fixed axis of rotation and then describe the experimental equipment. The measurements of the disk and cylinder motions during free oscillation are then described. The succeeding sections deal with measurements of the steady and unsteady aerodynamic moments which cause the motion. Detailed measurements have been made of the static and dynamic restoring moment, damping moment, the random unsteady moment produced by the turbulence and the effect of disturbances in the wake. The measurements are used to compute the mean-square amplitude of oscillation and to develop a qualitative model for the unsteady flow field in the wake that relates the turbulent moment to the vortex shedding process.

## 2. Theory for the oscillating motion

The problem of the oscillating motion of the disk or cylinder about a fixed axis can profitably be studied in the light of previous work on the response of mechanical or aerodynamic systems to turbulence. Lin (1943) studied the motion of a pendulum immersed in a turbulent stream. Liepmann (1952*a*) has considered the force exerted on an aerofoil in a turbulent stream. These problems were analysed using the same methods that were developed for the problems of excitation of a torsional balance by Brownian motion or the response of an electrical circuit to random noise. Liepmann (1952*b*) and Fung (1955) have given general discussions of these methods as used to understand the effects of turbulence on linear systems.

For the present investigation, we can write the approximate non-dimensional differential equation for the motion as

$$I_1^* \, d^2\theta/dt'^2 - C_{m\dot{\theta}} \, d\theta/dt' - C_{m\theta}\theta = C'_m(t'). \tag{1}$$

The equation and symbols are explained in detail in the appendix. The assumptions implicit in this equation are that the dimensionless unsteady aerodynamic moment acting on the body can be separated into three independent contributions representing damping, $C_{m\dot{\theta}} \, d\theta/dt'$; restoring moment, $C_{m\theta}\theta$; and turbulence, $C'_m(t')$. The damping and restoring moments are assumed to depend linearly on the angular velocity and position of the body, respectively, while the turbulent moments are assumed to be independent of the body motion and attitude. In practice this means that the body motion must be restricted to small angles and angular velocities and the turbulent moment must not be changed appreciably by the motion of the body.

## 3. Experimental apparatus

The experiments were conducted in the subsonic wind tunnel at the Aerospace Engineering Laboratories of the University of Michigan. This closed circuit tunnel has a 5 ft. by 7 ft. test section with continuously variable speed up to 225 ft./sec. The turbulence level in the test section is 0·1 % axially and 0·13 % transversely at 50 ft./sec. At 150 ft./sec the axial and transverse components

increase to 0·14 and 0·22 % respectively. A brief description of the experimental apparatus is given below. Further details are given by Willmarth & Hawk (1964).

For free-oscillation tests the models were supported with ball bearings mounted in two vertical struts fastened to the wind-tunnel walls. A few tests were made with disks supported by a knife-edge pivot mounted on a sting in the disk wake. The angular position of the models was determined with either of two light-sensitive systems. One system used two matched selenium photoelectric devices which were differentially illuminated when the model rotated. The other system

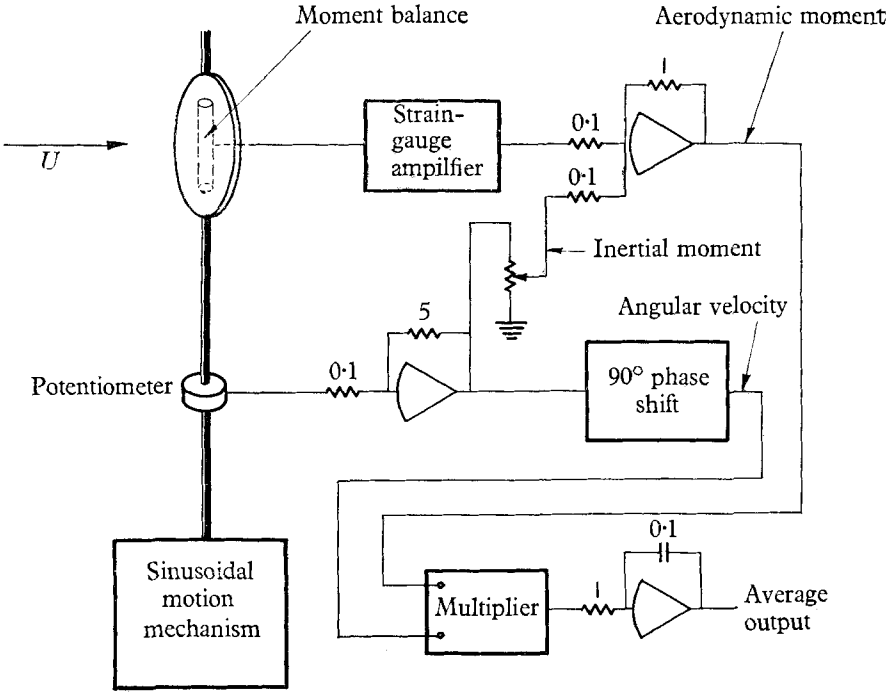


FIGURE 3. Schematic diagram of the experimental arrangement for forced-oscillation tests.

used a cadmium-sulphide photoconductive device in which the illumination was dependent on the angular orientation of the model. The models were made of various materials (brass, aluminium, magnesium, plywood, balsa wood and Styrofoam). The diameters varied from 0·33 to 1·83 ft.

Forced-oscillation tests of the unsteady aerodynamic moments were also made. Figures 2 (*a*) and 2 (*b*), plate 1, are photographs of the disk and cylinder mounted on the forced-oscillation supports. The heart of the forced-oscillation system was a dynamic-moment balance mounted inside the model. It consisted of a central cylinder, on which the model was mounted, that was surrounded by a hollow tube connected to the forced-oscillation mechanism. The central cylinder was fastened to the tube at each end by a flexure pivot formed by three crossed wires which prevented translation in any direction and rotation about two axes. Two small beams fitted with strain gauges prevented and detected rotation with respect to the hollow tube about the axis of the cylinder. The

strain-gauge bridge was driven and the output detected by a carrier-amplifier system.† The balance was calibrated and found linear over a range 0·01–4·0 ft.-lb. and was tested for 'interaction' with the maximum expected drag load (26 lb.). The drag-induced interaction moment was of the order of the minimum measurable moment, 0·01 ft.-lb.

The forced-oscillation tests were made with the aid of an analogue computer.‡ A schematic diagram of the basic circuit components is shown in figure 3. The sinusoidal model oscillations were produced by a scotch-yoke mechanism driven by a variable-speed hydraulic transmission.§

Other electronic equipment associated with these tests included an Ampex Model FR-1100 frequency-modulated tape recorder. In some cases data were recorded at $7\frac{1}{2}$ in./sec tape speed and played back at 60 in./sec tape speed, thereby increasing frequencies by a factor of 8. In this way power-spectral-density measurements at frequencies as low as 0·025 c/s could be made. A low-frequency variable-band-width wave analyser consisting of a narrow-band filter circuit with a centre frequency range from 0·2 to 160 c/s was used to obtain power spectra of the disk motion and the turbulent moment acting on the disk. A General Radio Model 736-A constant-band-width wave analyser was used for power-spectra measurement of the turbulent moment acting on the cylinder.

Electrical signals were monitored with a dual-beam oscilloscope and camera.‖ A Sanborn dual channel Twin-Viso Recorder was used to obtain oscillograph records of the low-frequency tests. A brief description of the more interesting analogue-computer circuits is given in this report when the particular measurements for which the circuits were designed are discussed. Detailed descriptions of the moment balance, electronic circuitry, and the special analogue-computer circuits are given by Willmarth & Hawk (1964).

## 4. Results and discussion of the disk experiments

The unsteady aerodynamics of the disk will be described first. The unsteady aerodynamic phenomena of the cylinder are similar to the disk phenomena, but additional complications are caused by motion of the line of separation on the cylindrical surface. The aerodynamics of the cylinder are described after some understanding of the disk aerodynamics is obtained. The experiments to be described include statistical analysis of free oscillations, static and dynamic measurements of aerodynamic restoring moment, measurements of the average and instantaneous damping moment during forced oscillations and studies of the effect of wake disturbances on the turbulent moment fluctuations.

### 4.1. *Free oscillations*

The general nature of the free oscillations about the statically-stable-equilibrium position with face normal to the flow is indicated by the oscillograph records of the motion shown in figure 1. Autorotation did not occur when a disk was initially

† Consolidated Elctrodynamics Corp. Amplifier system D.
‡ Applied Dynamics Model AD-1 electronic differential analyser.
§ Vickers, Inc., series TR 3.
‖ Tektronix models 502 and C-12.

at rest and the tunnel speed was slowly increased. Autorotation was observed if the disk was given an initial velocity while the tunnel was running. We have not studied the autorotation of disks, but Smith (1953) presents general considerations and results applicable to the autorotation phenomena.

### 4.2. *Frequency of oscillation*

The first tests showed that each disk oscillated continuously at a frequency dependent on wind speed and with an amplitude and phase which appeared to vary in a random manner. Figure 1, which gives amplitude–time records of two

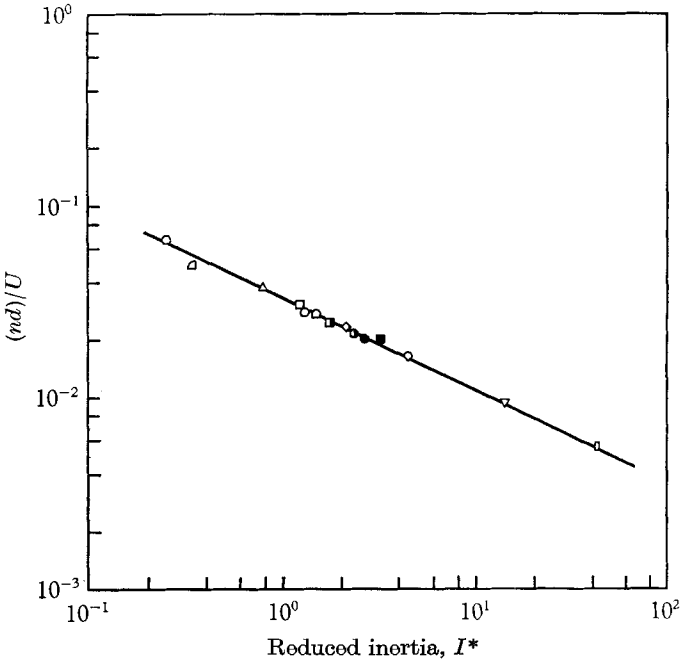


FIGURE 4. Dimensionless frequency as a function of dimensionless moment of inertia for free oscillations of disks. 68,000 < *Re* < 636,000.

| | *d* ft. | *h*/*d* | | *d* ft. | *h*/*d* |
|---|---|---|---|---|---|
| ○ | 0·5 | 0·0104 | △ | 0·92 | 0·0341 |
| ◑ | 0·5 | 0·0104 | ◇ | 0·92 | 0·0341 |
| ● | 0·5 | 0·0104 | ◿ | 0·42 | 0·0125 |
| □ | 1·0 | 0·0104 | ◺ | 0·42 | 0·0125 |
| ◧ | 1·0 | 0·0104 | ◇ | 0·42 | 0·0125 |
| ■ | 1·0 | 0·0104 | ▽ | 0·5 | 0·0416 |
| ◇ | 0·5 | 0·0104 | ▯ | 0·5 | 0·1250 |

disks, is typical. The average frequency of the oscillation was measured by simply counting the number of cycles in a given time. For a given model, $nd/U$ was nearly constant, varying slightly with Reynolds number *Re*, where $Re = Ud/\nu$. Figure 4 gives the relation between $nd/U$ and the reduced inertia, $I^* = I/\rho d^5$, for several disk models. In this figure $h$ is the disk thickness. As outlined in the appendix, the dimensionless frequency $nd/U$ of a second-order linear system with constant

restoring- and damping-moment coefficients should vary as $(I^*)^{-0.5}$. The experimental result (from figure 4) is that the dimensionless frequency varies as $(I^*)^{-0.44}$. This discrepancy is probably caused by a slight increase in effective dynamic restoring-moment coefficient as the dimensionless frequency of oscillation decreases.

### 4.3. *Static restoring moment*

The Styrofoam disk was clamped at fixed angles of attack and the average restoring-moment coefficient was measured with the moment balance and analogue computer. The measurements are displayed in figure 5 which shows an increase in restoring moment at higher Reynolds numbers. The same effect was

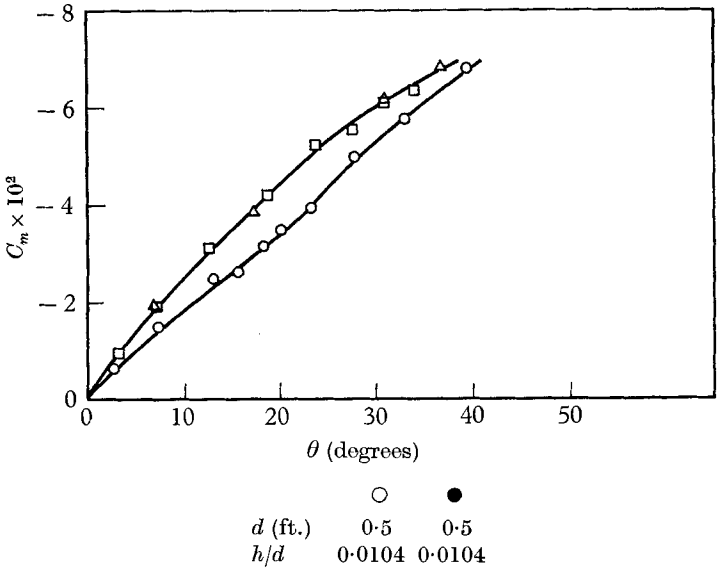


FIGURE 5. Static-moment coefficient of the Styrofoam disk, $d = 22$ in., $h/d = 0{\cdot}108$.

| | Reynolds no. | $(\partial C_m/\partial\theta)_{\theta=0}$ |
|---|---|---|
| ○ | $3{\cdot}61 \times 10^5$ | −0·126 per radian |
| △ | $5{\cdot}61 \times 10^5$ | −0·161 per radian |
| □ | $7{\cdot}21 \times 10^5$ | −0·161 per radian |

found in free-oscillation tests of a given disk. A slight increase in dimensionless frequency was observed in free oscillation tests of a given disk as the Reynolds number increased. The slope of the static-restoring-moment curve at $\theta = 0$, $C_{m\theta}$, is of the order of 30% greater in absolute value than the corresponding value of $C_{m\dot{\theta}}$ determined from free oscillation tests using (A 11). The static value of $C_{m\theta}$ is also considerably greater than the dynamic value of $C_{m\dot{\theta}}$ measured during forced oscillations. The measurement of $C_{m\dot{\theta}}$ during forced oscillations is discussed in §4.7 and was in agreement with the value obtained during free oscillations. We conclude that $C_{m\dot{\theta}}$ is lower than the static value when the disk is oscillating but is only weakly dependent on $nd/U$ in the range $10^{-2} < nd/U < 10^{-1}$.

### 4.4. *Damping of free oscillations*

From the linear theory for disk oscillations, see appendix, the rate of decay of transient oscillations is simply related to the amount of damping (in our notation $C_{m\dot{\theta}} < 0$ indicates damped motion). The determination of the damping from records of the rate of decay of free oscillations of disks that were displaced and released was severely hampered by the random-moment fluctuations which occurred during the damped motion. A large number of amplitude–time records were taken after release of the disk from an angular displacement varying from 20° to 40°.

We attempted to determine the logarithmic decrement from these records. The large amount of scatter present in the original data was reduced by averaging the logarithmic decrement from many tests for each individual disk. The average damping factor for the various disks was of the order of $C_{m\dot{\theta}} \simeq -0{\cdot}04$. The wide scatter made it impossible to determine the damping of the disks accurately from these tests. The magnitude of the damping-moment coefficients determined in this way is shown by the shaded region of figure 10.

### 4.5. *Statistical analysis of free oscillations*

The records of the disk motion were analysed statistically to determine the nature of the random oscillations and to determine the relationship of the disk motion to the unsteady aerodynamic phenomena that cause the motion.

Records of the disk motion were obtained from electrical signals produced by photoelectric and photoconductive systems illuminated by light whose intensity was modulated by the disk motion. The signals were recorded by an oscillograph and a frequency-modulated magnetic-tape recorder. Some of the signals contained very-low-frequency fluctuations, which were recorded at low tape speeds, $7\frac{1}{2}$ in./sec, and were later reproduced at 60 in./sec tape speed, thereby increasing the frequency by a factor of eight.

The probability distributions of the deflexion angle $\theta$ for a number of oscillating disks with different moments of inertia and at various wind speeds were determined using an analogue-computer comparator circuit. The mean-square amplitude (square of the standard deviation) was also determined with the analogue computer and was used to normalize the probability distribution for each disk.

The probability distributions for a typical disk mounted on a knife-edge pivot are shown in figure 6. It is apparent that the distributions are approximately Gaussian:

$$P(\theta) = \{1/\sqrt{(2\pi)}\} \int_{-\infty}^{\theta/\sqrt{\overline{\theta^2}}} \exp(-\gamma^2/2)\, d\gamma. \tag{2}$$

However, there are deviations from the Gaussian distribution for both small and large angles. The damping introduced by the type of pivot used to support the disk had a large effect on the root-mean-square amplitude of the motion but not on the normalized probability distribution. Results for other disks and pivots may be found in Willmarth & Hawk (1964). Higher root-mean-square amplitudes were obtained with the knife-edge pivot than with the best instrument-quality

ball bearings we could obtain. In fact, two tests with a knife-edge and ball-bearing pivot on the same aluminium disk with the same wind-tunnel conditions showed that the root-mean-square amplitude was 50 % greater with a knife-edge pivot. It is interesting to note that, if pivot friction is neglected, '$Q$' of the oscillating disk is only of the order of ten. Here $Q$ is defined as $2\pi$ times the ratio of the mean energy of the oscillating disk to the work done against aerodynamic damping per cycle.

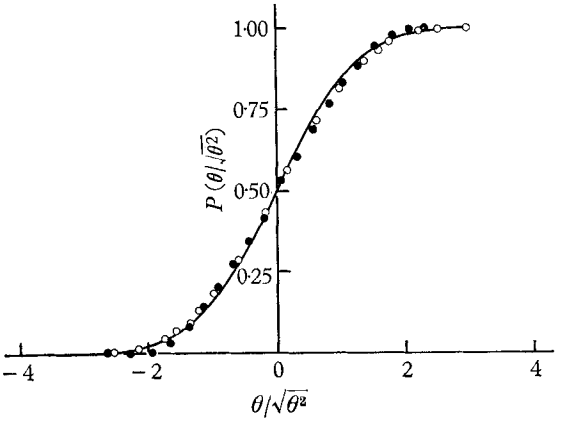


FIGURE 6. Measurements of the probability distribution of disk orientation angle $\theta$. ——, Gaussian distribution.

| | $\sqrt{\theta^2}$ | $U$ | $(nd/U) \times 10^2$ | Pivot |
|---|---|---|---|---|
| ● | 0·128 | 52·4 | 3·08 | K.E. |
| ○ | 0·122 | 100·0 | 3·05 | K.E. |

Close examination of the probability-distribution function for the disk angle with the knife-edge pivot shows that the large-amplitude oscillations are slightly less probable than one would expect for a Gaussian distribution. The deviations from the Gaussian distribution do not appear great enough to warrant further investigation. A more important problem is to gain understanding of the gross properties of the disk motion and aerodynamic phenomena.

A question that arose early in the investigation was: how can one decide whether the disk motion is influenced by flow fluctuations upstream of the disk? In order to determine the source of the unsteady moments that cause the motion, a number of different tests were made. We will discuss the tests that involve statistical observations of the motion of the disk in this section and reserve a description of the direct measurements of the unsteady aerodynamic exciting moment and the computation of the root-mean-square amplitude of oscillation for later discussion.

We made oscillograph and magnetic-tape records of the motion of a number of disks at various wind-tunnel speeds and analysed the probability density of the slowly varying amplitude of oscillation $\theta_0(t)$, where

$$\theta(t) \simeq \theta_0(t) \sin\{\omega t + \phi(t)\}. \tag{3}$$

Here $\theta_0(t)$ and $\phi(t)$, the phase angle, are assumed to vary slowly compared to $\omega t$. We analysed the oscillograph records of the amplitude and determined the

average amplitude of the envelope $\overline{\theta}_0$ and the probability density of the envelope amplitude,

$$(dP/d\theta_0)\,d\theta_0 = \text{probability that the envelope amplitude is between } \theta_0 \text{ and } \theta_0 + d\theta_0,$$

by measuring the average envelope amplitude with a planimeter and the probability density by counting the number of times a peak fell within a given range of amplitudes.† The analogue computer was also used to determine the probability distribution of the amplitude of the envelope $\theta_0(t)$. The signal representing the disk oscillation was rectified and passed through a second-order

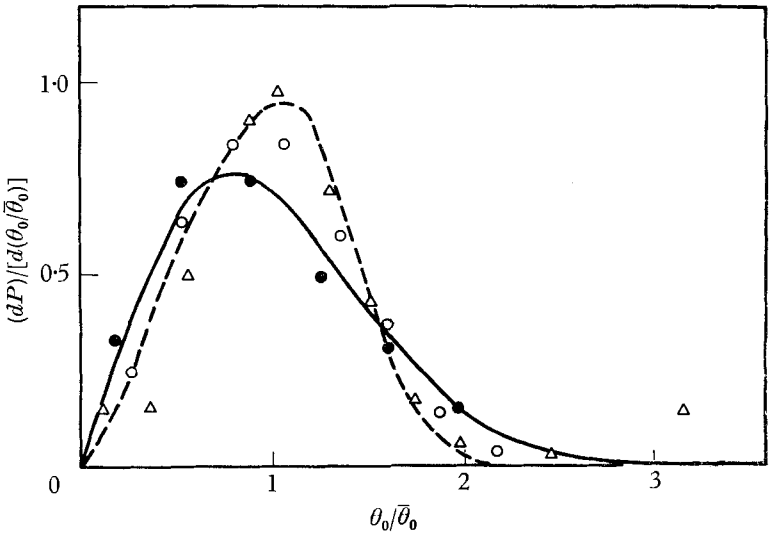


FIGURE 7. Comparison between various measurements of the probability density distribution of the slowly varying amplitude of oscillation $\theta_0$ for several disks. ——, Rayleigh distribution.

| | $\overline{\theta}_0 \times 10^2$ | Pivot | Grid | $(nd/U) \times 10^2$ | $Re \times 10^{-5}$ | $U$ (ft./sec) | $d$ (ft.) |
|---|---|---|---|---|---|---|---|
| △ | 4·22 | B.B. | None | 2·8 | 3·01 | 101·4 | 0·5 |
| ○ | 7·81 | B.B. | None | 3·35 | 1·71 | 24·8 | 1·0 |
| ● | 8·15 | B.B. | Yes | 3·35 | 1·71 | 24·8 | 1·0 |
| ——— | 14·6 | K.E. | None | 3·08 | 3·34 | 52·4 | 1·0 |

filter whose damping and frequency of resonance oscillation could be varied. By adjusting the filter by trial and error and comparing the filter output with the peaks of the input signal, an acceptable reproduction of the function $\theta_0(t)$ was obtained. The probability distribution of the signal representing $\theta_0(t)$ was then determined using a comparator circuit. The results of these measurements are shown in figure 7.

The measurements of the probability distribution of $\theta_0$ can be compared with the Rayleigh-distribution function:

$$P(\theta_0/\sqrt{\overline{\theta_0^2}}) = \text{probability of a smaller value of } \theta_0/\sqrt{\overline{\theta_0^2}} = 1 - \exp(-\theta_0/\sqrt{\overline{\theta_0^2}}), \qquad (4)$$

† We are indebted to Mr T. Ishii for suggesting this measurement.

which represents the probability distribution of the amplitude of the output of a narrow-band linear system subjected to a Gaussian input (see Davenport & Root 1958). In order to compare measurements from the analogue computer, in which $\overline{\theta_0^2}$ was measured, with those taken by hand, in which $\bar{\theta}_0$ was measured, we have normalized the data using the mean amplitude of the envelope $\bar{\theta}_0$ and have re-cast the Rayleigh-probability-density function (from (4)) in the form

$$dP(\theta_0/\bar{\theta}_0)/d(\theta_0/\bar{\theta}_0) = (2/\pi)\,(\theta_0/\bar{\theta}_0)\exp\{-(\pi/4)\,(\theta_0/\bar{\theta}_0)^2\}, \tag{5}$$

using the fact that $\bar{\theta}_0 = \sqrt{(\pi\overline{\theta_0^2}/2)}$. The comparison between the measurements is shown in figure 7. It is clear that the measured probability-density functions agree with each other but not with the Rayleigh distribution.

One test was made with a 5 ft. × 7 ft. turbulence grid installed in the tunnel ahead of the model. The grid was made from wooden rods $\frac{1}{4}$ in. in diam. on centre lines spaced $1\frac{1}{4}$ in. apart and was placed 87 in. upstream of the disk. The average amplitude of disk oscillation was not appreciably affected by the grid, but the probability density of the envelope amplitude $\theta_0$ was altered. The results of the probability-density measurement for this case are also shown in figure 7. The probability density is approximately the same as the Rayleigh probability density. We may say that the exciting moment acting on the disk has been altered by the grid in such a way that the average amplitude of the envelope is not changed but large and small values of $\theta_0$ are more probable while intermediate values of $\theta_0$ are less probable. It appears that the intense free-stream turbulence distorts the turbulent eddies in the wake and produces a statistical distribution of the random turbulent moment $M'$ that is very nearly Gaussian.

We also measured the power spectral density of the envelope amplitude $\theta_0(t)$ for a number of disks when no grid was installed in the tunnel. The results of the measurements were approximately corrected for variable band width of the wave analyser, normalized, and plotted in non-dimensional form in figure 8. The spectral density in this figure is defined by

$$f_{\theta_0}(\omega) = (2/\pi)\int_0^\infty \overline{\theta_0(t)\,\theta_0(t+\tau)}\cos\tau\,d\tau. \tag{6}$$

The data show that the power spectra of $\theta_0(t)$, which must depend on the statistical properties of the exciting moment, scale with the characteristic time $d/U$. The spectra show considerable scatter at low frequencies but this may be the result of insufficient averaging time, the lowest frequencies (in real time) were of the order of 0·02 c/s.

The result that with disks of different diameters the power spectrum of the amplitude of the disk motion scales with the disk diameter means that the exciting moment is produced by turbulence in the disk wake which must have a length scale dependent on the disk diameter and a time scale dependent on $d/U$. It is not likely that ordinary turbulence levels in the tunnel have any appreciable affect on the disk motion but more severe turbulence produced behind a grid approximately 7 disk diameters upstream had a marked effect on the probability density of the disk motion. We conclude that the disk exciting moment is caused by an unsteady torque produced by wake turbulence whose statistical properties

but not intensity (in this one case) can be altered by intense small-scale turbulence originating upstream. The effect of downstream disturbances in the disk wake will be discussed in a later section.

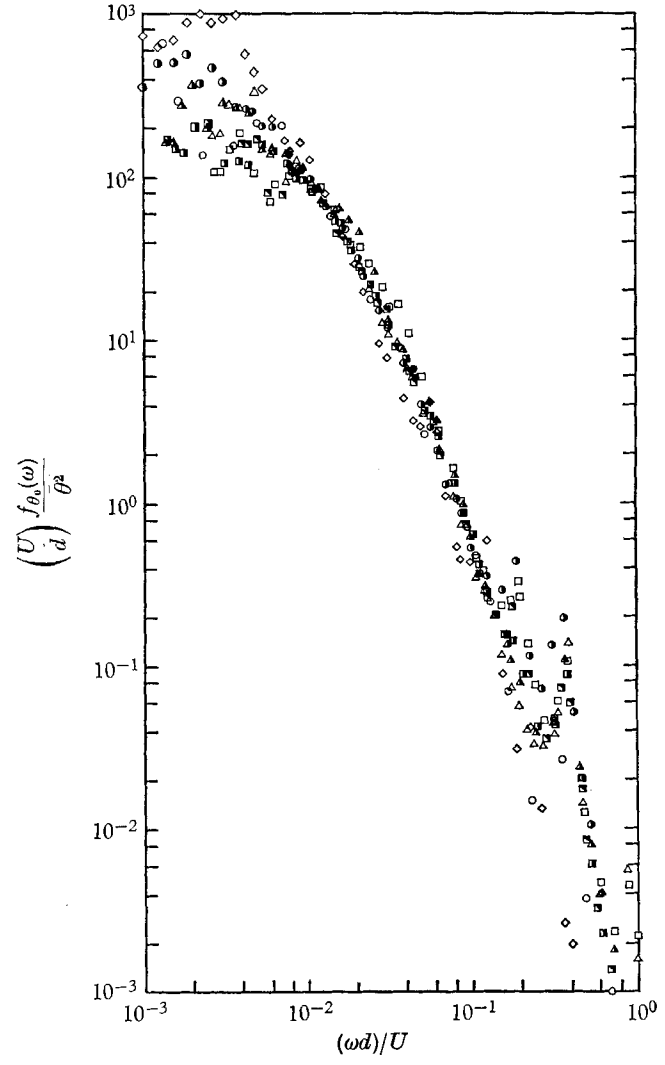


FIGURE 8. Power spectra of the slowly varying amplitude of oscillation $\theta_0$ for several disks.

| | Diam (ft.) | $h$ (in.) | $U$ (ft./sec) | $(nd/U) \times 10^2$ | Pivot |
|---|---|---|---|---|---|
| ○ | 0·5 | 0·0625 | 53·7 | 3·02 | B.B. |
| ◑ | 0·5 | 0·0625 | 101·4 | 2·81 | B.B. |
| △ | 1·0 | 0·125 | 52·4 | 3·09 | K.E. |
| ▲ | 1·0 | 0·125 | 102·3 | 3·05 | K.E. |
| □ | 1·0 | 0·125 | 52·0 | 3·10 | B.B. |
| ◥ | 1·0 | 0·125 | 35·6 | 3·04 | B.B. |
| ◧ | 1·0 | 0·125 | 99·9 | 3·00 | B.B. |
| ◇ | 0·5 | 0·250 | 102·0 | 0·95 | B.B. |

### 4.6. *Forced oscillation tests*

To study the aerodynamic moment caused by the disk motion, we forced the disk to oscillate sinusoidally and measured the fluctuating moment acting on the disk with the moment balance. Figure 2 (*a*), plate 1, is a photograph of the disk mounted on the forced-oscillation supports. We used analogue-computer elements (see figure 3) to subtract the inertial moment of the disk from the moment measured by the balance. The resulting aerodynamic moment was processed with the analogue computer to remove the turbulent moment. We also used the computer to determine the instantaneous work rate, the average damping coefficient and some features of the turbulent moment.

### 4.7. *Dynamic moment and work rate*

The disk was forced to oscillate sinusoidally with various amplitudes at frequencies ranging from 2 to 6 c/s and wind speeds from 25 to 100 ft./sec. The disk was made from Styrofoam plastic, a light, rigid material and was 2·25 in. thick (to accommodate the moment balance) and 22 in. in diameter. The dimensions and weight of material (including epoxy and resorcinol adhesives) were used to compute the moment of inertia of the disk.

The measurements of the aerodynamic moment and work rate were made using a sample and hold circuit. The analogue computer continuously determined the disk moment and the rate at which work was done by the disk on the air in the wind tunnel (see figure 3). At a certain phase of the oscillation the instantaneous aerodynamic-moment or work-rate signal was sampled and fed into an integrator. The signal in the integrator from many samples obtained at the same phase of oscillation gave the average dynamic moment or work rate at that position.

The results of a typical test are shown in figures 9 (*a*) and 9 (*b*). In this test the disk was provided with a sharp edge by fastening a cardboard sheet, 26 in. diameter, on the front face. An oscilloscope trace of the aerodynamic moment and disk position is shown in figure 9 (*a*). In figure 9 (*b*) the averaged instantaneous aerodynamic-moment coefficient

$$C_m = M/qSd \tag{7}$$

is shown along with the averaged instantaneous rate of work done by the fluid on the disk

$$C_{\dot{w}} = C_m \dot{\theta} d/U \tag{8}$$

as a function of the phase $\omega t$. The average aerodynamic moment coefficient in figure 9 (*b*) is approximated very well by the expression

$$C_m(t) = -0{\cdot}049 \sin(\omega t + \phi), \quad \phi = 21°. \tag{9}$$

(A 2) can be written in dimensionless form with $M'(t) = 0$:

$$C_m(t) = C_{m\theta}\theta(t) + C_{m\dot{\theta}}\dot{\theta}(t). \tag{10}$$

Comparison of (9) and (10), where $\theta = 0{\cdot}425 \sin \omega t$, yields

$$C_{m\theta} = -0{\cdot}108, \quad C_{m\dot{\theta}} = -0{\cdot}105. \tag{11}$$

Many other tests with the 2·25 in. thick Styrofoam disk without the cardboard edge on the front face showed similar records of averaged aerodynamic moment but with curious fluctuations superimposed on the basic sinusoidal moment.

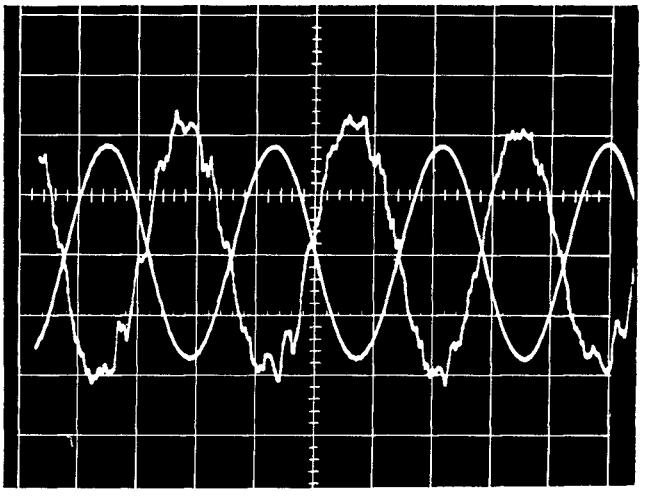

(*a*)

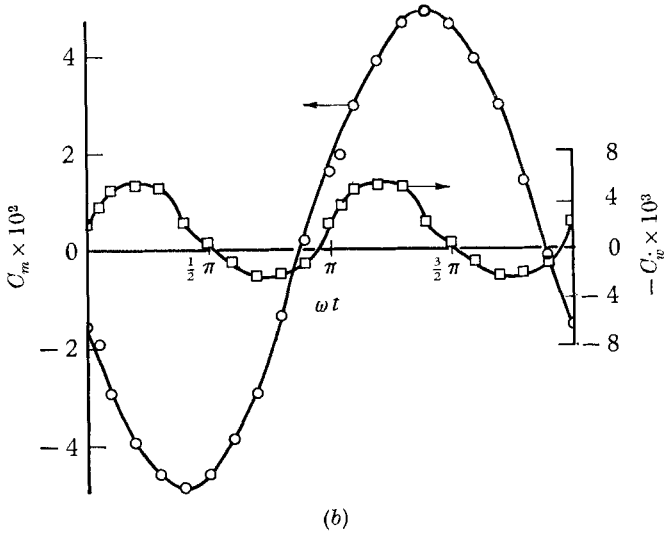


(*b*)

FIGURE 9. (*a*) Oscilloscope traces of orientation angle $\theta$ and the aerodynamic moment during forced sinusoidal motion. (*b*) Average aerodynamic-moment and work-rate coefficients during one cycle of forced sinusoidal oscillation. Styrofoam disk with $d = 26$ in., $h = \frac{1}{16}$ in., cardboard disk mounted on upstream face. $\theta_0 = 0{\cdot}425$ rad, $\omega = 11{\cdot}3$ rad/sec, $U = 65{\cdot}4$ ft./sec, $Re = 11{\cdot}8 \times 10^5$, $nd/U = 5{\cdot}96 \times 10^{-2}$.

The fluctuations were the result of flow separation and re-attachment at the disk edges. We noticed that the basic sinusoidal character of the oscillating aerodynamic moment was destroyed at large amplitudes of oscillation, $\theta > 45°$. In order to determine $C_{m\dot{\theta}}$ when the disk did not have a sharp edge, we used the

analogue computer to measure the average of the rate of work done by the fluid on the disk:

$$\overline{W} = (1/T)\int_0^T M(t)\,\dot{\theta}(t)\,dt. \tag{12}$$

We assumed that the moment $M$ could be represented by (A 2) and used the facts that for the measurements $\theta = \theta_0 \sin \omega t$, the turbulent moment had zero mean, and $T$ was large to obtain

$$\overline{W} = (\partial M/\partial\theta)_{\theta+0}\,T^{-1}\int_0^T \theta\dot{\theta}\,dt + (\partial M/\partial\dot{\theta})_{\dot{\theta}=0}\,T^{-1}\int_0^T \dot{\theta}^2\,dt = (\partial M/\partial\dot{\theta})_{\dot{\theta}=0}\,\theta_0^2\omega^2. \tag{13}$$

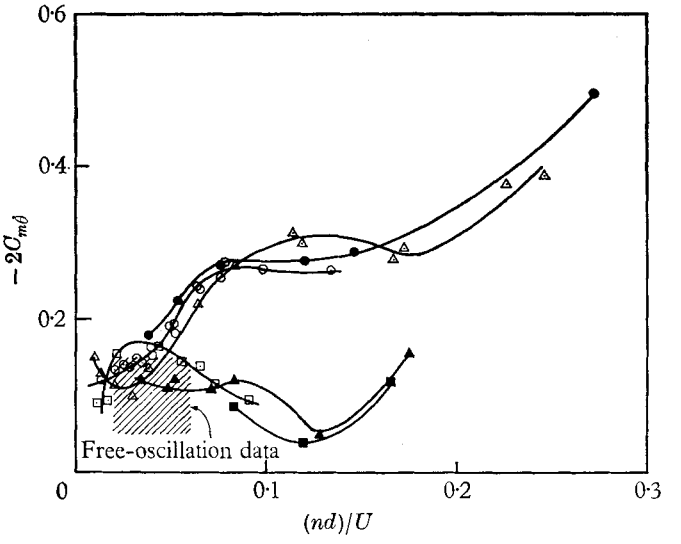


FIGURE 10. Measurements of the damping-moment coefficient during forced oscillations of disks. Values of $\theta_0$ (rad): △, 0·15; ⊙, 0·42; □, 0·71; ●, 0·41; ■, 0·70; ▲, 1·0.

Using the measured value of $\overline{W}$, (13) and (A 7) the value of $C_{m\dot{\theta}}$ is

$$C_{m\dot{\theta}} = \overline{W}U/\theta_0^2\omega^2 qSd. \tag{14}$$

The results of damping measurements made at different amplitudes and dimensionless frequencies are displayed in figure 10. In these results one should realize that the decomposition of the moment proposed by (A 2) is not valid for $\theta_0 > 0{\cdot}5$ radians and may also fail for large dimensionless frequencies of oscillation, $nd/U > 0{\cdot}15$; however, one can easily recover $\overline{W}$ using (14) if necessary. Additional analysis of the results for large amplitude and frequency are given by Willmarth & Hawk (1964). It should be noted that in all our free-oscillation tests the frequency and amplitude were small, $nd/U < 0{\cdot}1$ and $\sqrt{\overline{\theta^2}} < 0{\cdot}13$ radians respectively. The moment decomposition of (A 2) and results of figure 10 are a good approximation for the case of free oscillations.

The damping-moment coefficients measured from the decay of free oscillations (see figure 10) are generally lower (but have larger scatter) than the forced-oscillation damping-moment coefficients. The most probable explanation for the difference is the fact that in measuring the rate of decay of free oscillations one is

attempting to measure the rate at which the disk loses energy while the turbulent exciting moment is adding energy to the free oscillations during the measurements. In the forced-oscillations tests the moments are measured during periodic, constant-amplitude oscillations, and the effects of the turbulent moment can be removed if one assumes that the turbulent-moment fluctuations are uncorrelated with disk motion, i.e. $\overline{M'\dot{\theta}} = 0$.

The Reynolds number, which varied from $0{\cdot}2 \times 10^6$ to $1{\cdot}3 \times 10^6$ for the measurements of $C_{m\dot{\theta}}$ shown in figure 10, had very little effect on the results. When

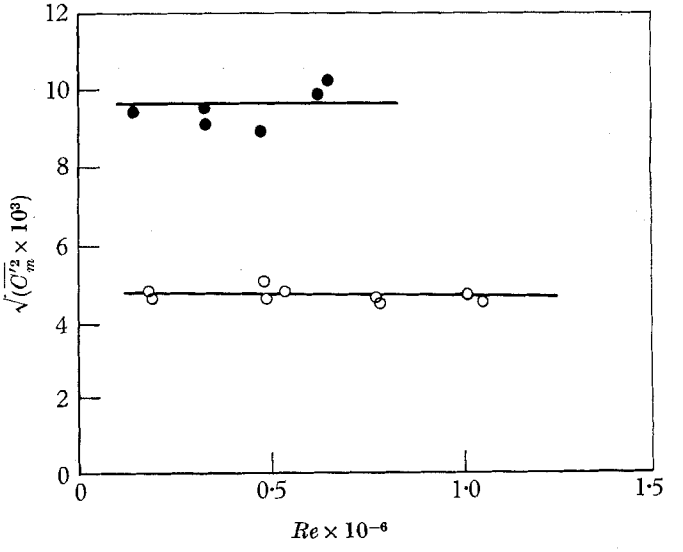


FIGURE 11. Root-mean-square moment coefficients for the Styrofoam disk and cylinder with face normal to the flow, $\theta = 0$. ●, cylinder; ○, disk.

$nd/U > 0{\cdot}06$ there is a marked increase (as much as a factor of 10) in $C_{m\dot{\theta}}$ for oscillation amplitudes greater than 0·7 radian. This increase is connected with non-linear behaviour of the aerodynamic moment. We did not find any case in which the damping-moment coefficient (or $\overline{W}$, the average rate of work done on the disk by the fluid during forced oscillations) became positive. We originally thought that at large amplitudes ($\theta_0 \simeq 1$ radian was the maximum amplitude our driving mechanism could produce) $\overline{W}$ would become positive and would help explain the mechanism of autorotation. We now understand that to start disk autorotation sufficient rotational energy must be supplied to turn the disk face nearly parallel to the stream. In this position the disk is statically unstable and probably gains sufficient energy from the destabilizing moment produced when there is little flow separation to carry it on into autorotation.

### 4.8. *The buffeting moment produced by turbulence in the wake*

We investigated some features of the buffeting moment produced by turbulence in the wake of the disk. The investigation included measurements of the fluctuating moment acting on the disk and the correlation between the moment and velocity on the disk-face when the disk was clamped with face normal to the

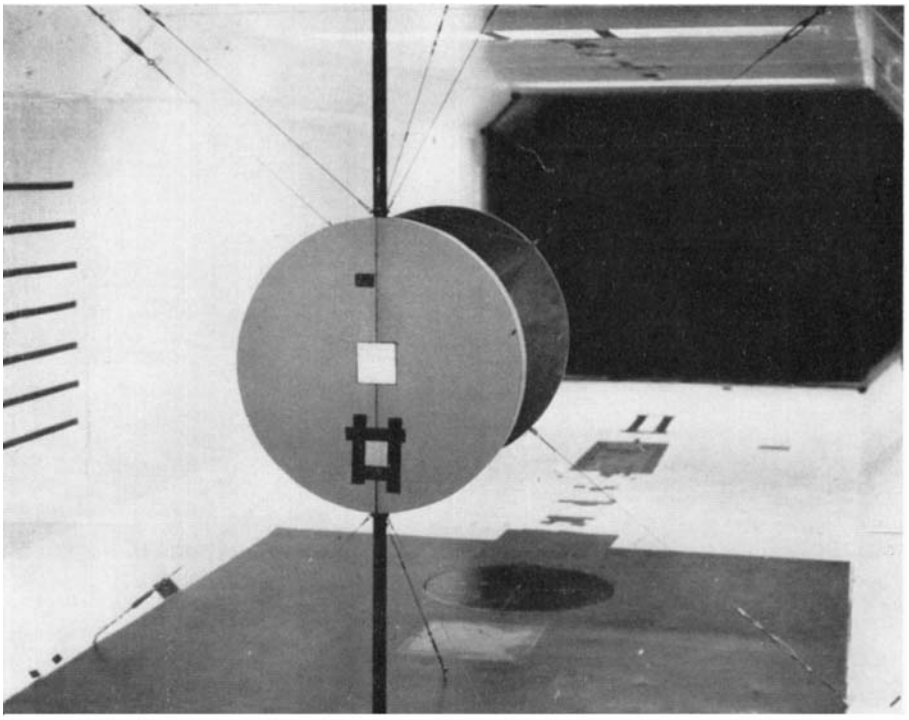

(*a*)

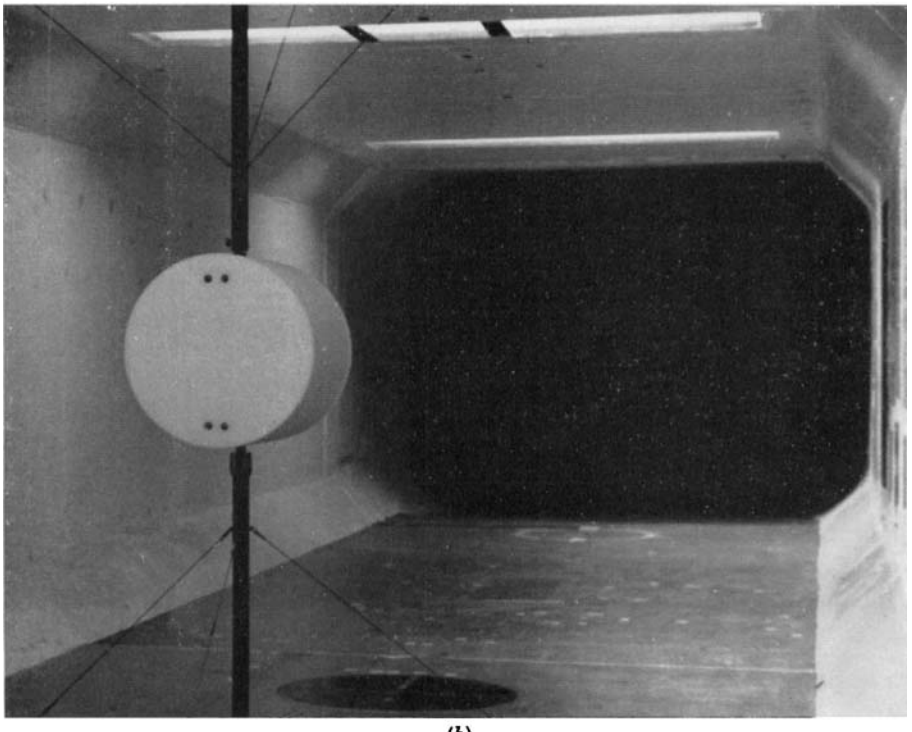

(*b*)

FIGURE 2. (*a*) 22 in. diameter Styrofoam disk mounted in the tunnel on forced-oscillation supports with a fixed 22 in. plywood disk downstream. (*b*) 11·65 in. diameter Styrofoam cylinder mounted in the tunnel on forced-oscillation supports.

stream. Tests were also made with a splitter plate or another disk placed in the disk wake.

The root-mean-square moment coefficient $\sqrt{C_m'^2}$ for a single disk is displayed in figure 11. $\sqrt{C_m^2}$ is constant in the range $10^5 < Re < 10^6$. The spectrum of the turbulent moment

$$f_m(\omega) = (2/\pi)\int_0^\infty \overline{M'(t)\,M'(t+\tau)}\cos\omega\tau\,d\tau \tag{15}$$

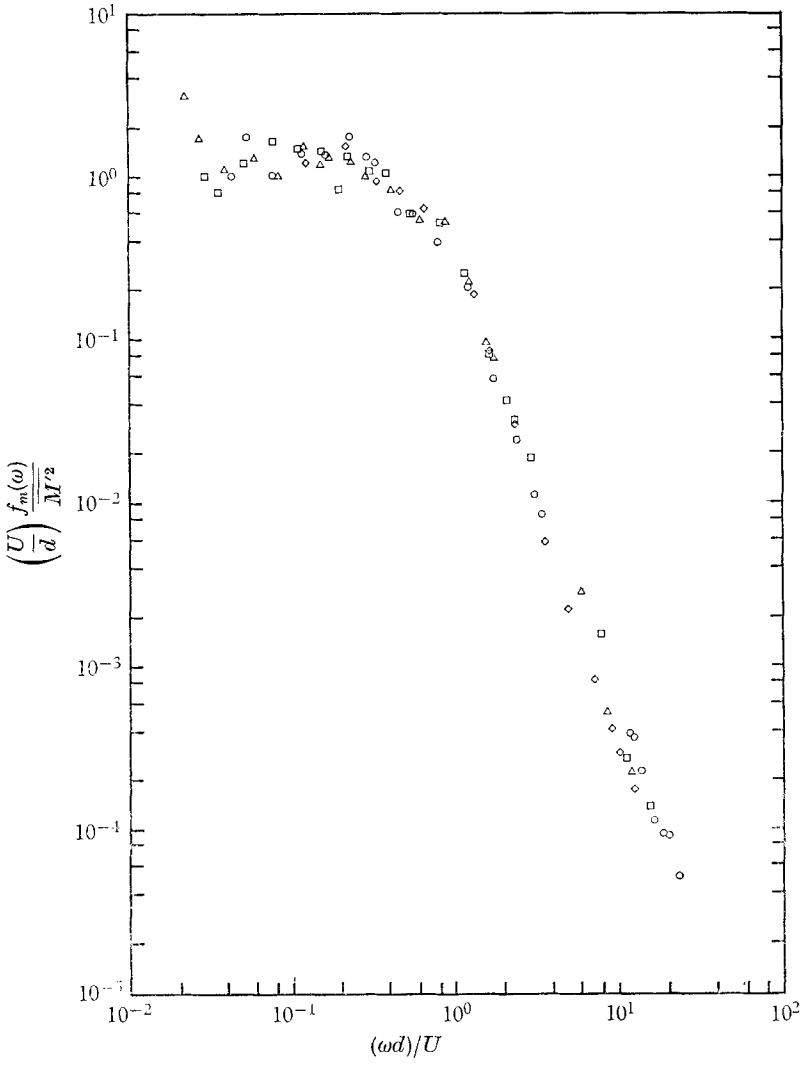


FIGURE 12. Dimensionless power spectra of the fluctuating aerodynamic moment acting on the Styrofoam disk with face normal to the flow, $\theta = 0$.

| | $\sqrt{C_m'^2} \times 10^3$ | $Re \times 10^{-5}$ |
|---|---|---|
| ◇ | 4·76 | 1·87 |
| ○ | 4·77 | 5·33 |
| □ | 4·43 | 7·82 |
| △ | 4·49 | 10·50 |

is displayed in figure 12 in terms of dimensionless parameters obtained from the characteristic time $d/U$. We have discussed (§ 4.5) the fact that the spectra of the amplitude of free oscillations, $\theta_0(t)$, also scale with the characteristic time $d/U$. The moment and motion must therefore be caused by moment fluctuations which also scale with the time $d/U$. In the discussion below, we will demonstrate how flow disturbances in the wake change the moment fluctuations acting on the disk.

### 4.9. *Effect of a fixed disk in the wake*

We made a number of tests with a fixed plywood disk $\frac{3}{4}$ in. thick and 22 in. in diameter placed in the wake of the Sytrofoam disk containing the moment balance. The plywood disk was mounted on a rod supported by wires running to the tunnel walls.

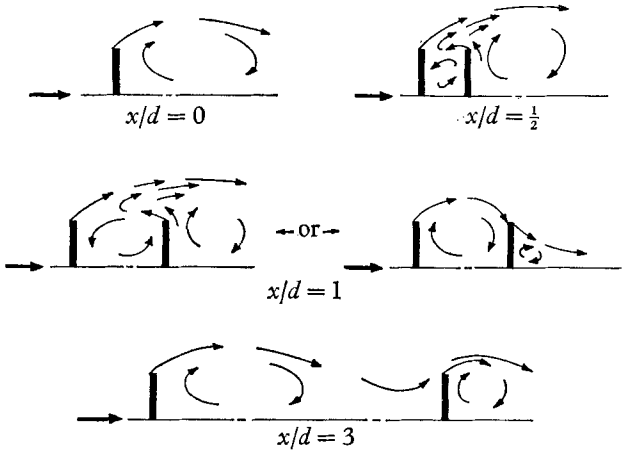


FIGURE 13. Sketch of the mean-flow direction revealed by tufts of yarn in the meridian plane of the disk wake when a second disk is placed a distance $x$ downstream of the first. $Re = 6 \times 10^5$.

Observations of the flow field at Reynolds number $6 \times 10^5$ with variable spacing between the disks (obtained by sliding the plywood disk along the rod) were made with tufts of woollen yarn fastened to the disks and to a network of wires in a meridian plane in the wake. The nature of the average flow field in the wake is shown in the sketches of figure 13. When $x/d \simeq 0$, where $x$ is the distance between the front faces of the disks, there is a general circulation of air in the wake upstream along the axis and downstream along the shear layer that springs from the edge of the disk. When $0 < x/d < 1$ there is, behind the rear disk, the same general circulation upstream along the axis and downstream along the shear layer, observed with $x/d = 0$, but between the two disks there is a reverse downstream circulation of air along the axis that is caused by an upstream flow of air over the edge of the rear disk into the outer part of the region between the disks.

When $x/d \simeq 1$, transition of the flow field between that found above for $0 < x/d < 1$ and that found with $x/d > 1$ was observed. The new régime of flow for $x/d \simeq 1$ does not have upstream flow of air over the edge of the rear disk. Instead a single, unsteady, annular vortex is trapped between the disks. This

trapped vortex-type flow fluctuated rather violently. Whenever the trapped vortex régime appeared, the annular region bounded by the free shear layer appeared to contract after passing over the trapped vortex and partially reattach at the edge of the rear disk. The mean flow field resembles a three-dimensional analogue of the classical two-dimensional Riabouchinsky flow (Birkhoff & Zarantonello 1957) between two parallel plates set normal to the stream. It was not possible to predict which flow field would be observed at the spacing $x/d \simeq 1$. Sometimes one flow field or the other would persist for an hour or more after starting the tunnel. Larger spacing between the disks resulted in two separate flow fields about each disk similar to that observed about a single disk.

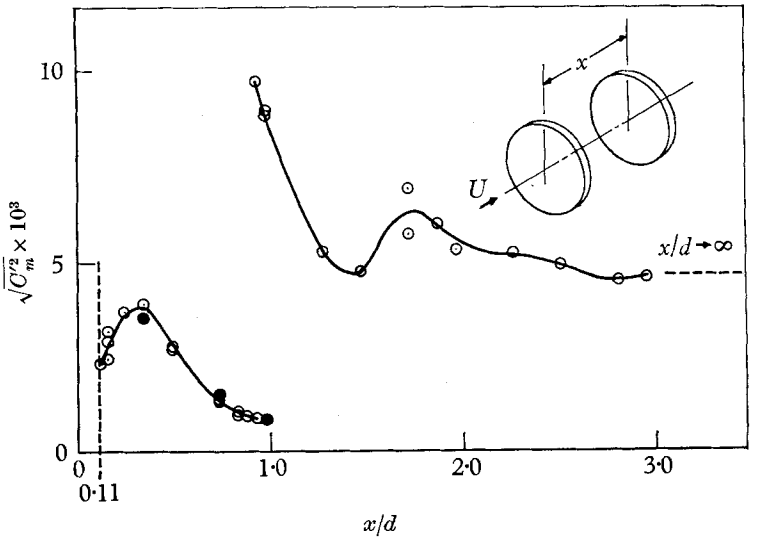


FIGURE 14. The root-mean-square moment coefficient acting on a disk when a second disk is placed a distance $x$ downstream of the first. ⊙, $Re = 0{\cdot}6 \times 10^6$; ●, $Re = 1{\cdot}2 \times 10^6$.

The root-mean-square moment acting on the forward disk was measured for various values of $x/d$. The results are displayed in figure 14. The smallest value of $x/d$ ($x/d = 0{\cdot}11$) corresponds to a small gap (0·20 in.) between the front and rear disks. Here $x$ is the distance between the front faces of the two disks. At this position the rear face of the front disk is partially shielded from pressure fluctuations in the wake and the root-mean-square moment fluctuations are (coincidentally) one half the value obtained when $x/d \to \infty$. As the disk spacing increases the moment fluctuations increase somewhat and then fall to $\frac{1}{5}$ of their value for $x/d \to \infty$. When $x/d$ was about equal to one, we were very fortunate during one run to observe the flow in first one state and then the other for a long enough period (2 min) to obtain measurements of $\sqrt{C_m'^2}$ in both states. The moment fluctuations increased by an order of magnitude in the flow régime with a trapped vortex. Oscillograph records of the moment fluctuations in the trapped vortex régime revealed a definite periodicity of large amplitude when $x/d = 1$. This periodicity was observed only at $x/d = 1$. We measured the lower-level moment fluctuations at $Re = 0{\cdot}6$ and $1{\cdot}2 \times 10^6$ but made all our measurements of $\sqrt{C_m'^2}$, for $x/d > 1$, at $Re = 0{\cdot}6 \times 10^6$.

We also measured the correlation between the fluctuating moment $M'$ and the fluctuating radial velocity $u'$ on the disk face. The radial velocity was measured with a hot wire 0·07 in. from the disk face and 5 in. from the centre of the disk along a radial line oriented in the direction reckoned positive in the direction of the vector $\mathbf{U} \times \mathbf{M}'$. That is to say $u'$ is counted positive if there is an increase in radial velocity outwards from the disk centre along this radial line. The measured correlation $\overline{u'M'}/\sqrt{\overline{u'^2}}\sqrt{\overline{M'^2}}$ was positive for any spacing between the disks. There was a large increase in the correlation (from 0·3 to 0·8) when $x/d$ approached one. This was followed by a sharp decrease and gradual rise to the value (0·36) found when $x/d \to \infty$. The significant observation contained in the results of the correlation measurements is the fact that $\overline{u'M'} > 0$.

### 4.10. *Model for the fluctuating flow field*

We would like to propose a simple model for that part of the fluctuating flow field responsible for the moment fluctuations acting on the disk. The facts that must be explained by the model are:

(i) The fluctuating moment is produced by flow fluctuations in the wake and the spectra of the fluctuating moment scales with the characteristic time $d/U$.

(ii) The moment fluctuations vary in magnitude when there is a fixed disk in the wake. The moment fluctuations are large when there is a fluctuating trapped vortex between the disks, $x/d = 1$. When there is a weaker vortex between the disks, $x/d \simeq 1$, the moment fluctuations are smaller.

(iii) The moment fluctuations and the velocity fluctuations on the front of the disk are correlated.

(iv) The correlation $\overline{M'u'}$ is positive.

A rough explanation of the phenomena may be made if we assume there is an unsteady annular vortex filament in the turbulent wake just behind the disk. The annular vortex is a result of air circulation in the wake upstream along the axis, radially outward over the rear face of the disk, and downstream along the shear layer. The annular vortex is driven by the flow in the shear layer springing from the edge of the disk. At random times the wake vortex is disturbed and a portion of the annular vortex filament is carried away by the higher-speed air in the shear layer. The flow field is three-dimensional, and there is no preferred location along the periphery of the shear layer for the shedding of a portion of the vortex filament. When shedding occurs at a given azimuthal position, the annular vortex filament is elongated at this position and there is a deflexion and an increase (caused by vortex stretching) in the back flow upstream along the axis as fluid in the wake is induced (by the vortex flow field) to flow into the region near the periphery of the disk formerly occupied by the shed portion of the vortex filament. The increased velocity and outward deflexion of upstream flow along the axis in the wake cause a momentary increase in pressure on the rear face of the disk on that portion nearest the location of the shed vortex filament and perhaps a decrease in wake pressure on the opposite side of the disk. (It may be helpful to visualize an upstream wake flow which produces a rear stagnation region that is moved about by vortex shedding.) The pressure fluctuations behind the disk also disturb the shear layer, which bulges outward on one

side (near the shed portion of the annular vortex) and inward on the other side thereby causing an increase in the radial velocity on the front of the disk at a point diametrically opposite the location of the shed vorticity along the periphery of the shear layer. From this model it can be understood that, if the moment fluctuation is produced primarily by pressure changes *behind* the disk, the result $\overline{M'u'} > 0$ ((iv) above) is explained. It must be noticed that the perturbation of the potential flow over the front face of the disk caused by the deflexion of the shear layers would produce a moment with sign opposite to the moment produced by the pressure perturbation in the wake that is responsible for the original shear layer deflexion. One must simply argue that the pressure changes in the wake behind the disk have a greater ability to produce moment fluctuations than the resulting (and opposite) moment fluctuations produced by the potential flow on the front of the disk.

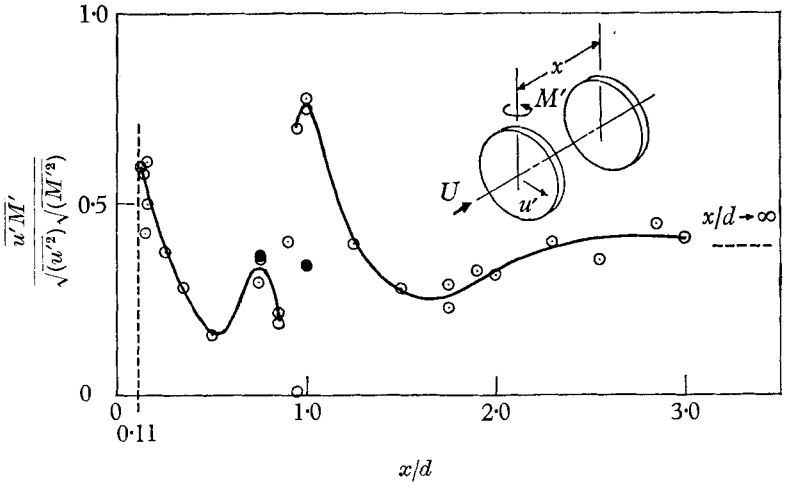


FIGURE 15. The correlation between the fluctuating disk moment and radial velocity on the disk face when a second disk is placed a distance $x$ downstream of the first. ⊙, $Re = 0{\cdot}6 \times 10^6$; ●, $Re = 1{\cdot}2 \times 10^6$.

With this model we can explain the increase in moment fluctuations observed when a fixed disk is placed in the wake of another with a spacing $x/d = 1$. The trapped vortex between the disks may be somewhat stronger and more coherent because it is restrained by the rear disk. The shedding process should induce more intense pressure fluctuations in the wake because the shed vorticity (which is of greater strength) must pass over the edge of the fixed disk and protrude farther out into the shear layer where it is subjected to an increased rate of vortex stretching.

This model also suggests that the aerodynamic damping of the oscillating disk is a result of the motion and configuration of large eddies in the wake. We do not have any further observations to lend quantitative support to the model. We believe that further work (particularly studies to correlate the phase shift of the undamped static restoring moment, see (10), with the wake pressure and flow field) in an attempt to verify or refute this model might be fruitful.

### 4.11. *Effect of a splitter plate in the wake*

Tests were made with a fixed splitter plate of variable length $l$ mounted behind the disk. The splitter plate extended between the top and bottom walls of the tunnel in the plane defined by the pivot axis of the disk and the stream direction. The upstream edge of the plate was as close as possible to the rear face of the disk but the gap was not sealed.

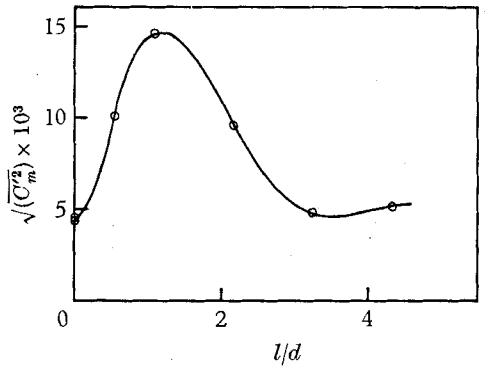


FIGURE 16

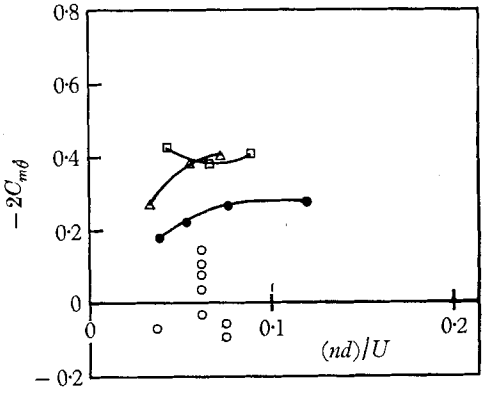


FIGURE 17

FIGURE 16. The root-mean-square moment coefficient acting on a disk when a splitter plate of length $l$ is placed in the wake parallel to the moment axis.

FIGURE 17. Measurements of the damping-moment coefficient $C_{m\theta}$ during forced oscillations of a disk with a splitter plate of length $l$ in the wake.

| | $l/d$ | $\theta_0$ (rad) |
|---|---|---|
| ● | 0 | 0·41 |
| ○ | 1·09 | 0·41 |
| △ | 2·18 | 0·41 |
| □ | 3·27 | 0·41 |

Figure 16 shows the root-mean-square moment fluctuations acting on a fixed disk. As the splitter-plate length increases, the moment fluctuations reach a maximum near $l/d = 1$ and then fall to the values near those obtained for $l/d = 0$. This result is qualitatively similar to the result found with a fixed disk in the wake. We did not have time to make tests with longer splitter plates to discover what value the root-mean-square moment fluctuations would attain for large $l/d$. We would like to suggest that the large increase in the moment fluctuations for $l/d = 1$ may be caused by separation of the fluctuating upstream wake flow (produced during vortex shedding) from the downstream end of the splitter plate.

The forced-oscillation damping-moment coefficient acting on the disk with a splitter plate in the wake was also measured. The experimental procedure and data reduction were the same as already described for the isolated disk (see (14)). The results of the measurements are shown in figure 17 for various-length splitter plates. When the splitter-plate length was equal to the diameter, the damping coefficient measurements had large scatter. The averaging time for

these measurements was of the order of one minute. The scatter suggests that the wake flow field may have two possible configurations with transition from one to the other occurring during the time of measurement.

The measured damping-moment coefficients were positive for splitter-plate length equal to disk diameter. In addition the root-mean-square turbulent moment is large (see figure 16). This suggests that a freely oscillating disk with splitter plate in the wake should exhibit divergent oscillations if the splitter plate is of the proper length, $l \simeq d$. For longer splitter plates, $l > d$, the damping moment coefficient became more negative than the value measured with no splitter plate. The amplitude of free oscillations for a disk with a long splitter plate, $l/d > 3$, should therefore be lower than that for an isolated disk. (The root-mean-square moment acting on the disk with a long splitter plate, $l/d > 3$, is almost the same as that on a disk with no splitter plate, see figure 16.)

### 4.12. *The computation of the root-mean-square deflexion angle*

Implicit in the formulation of the problem of disk oscillations as the response of a linear system to a Gaussian, random forcing function (see § 2) is the fact that the root-mean-square response can be computed if the power spectrum of the forcing function and the properties of the system are known. The theory is discussed from a mathematical point of view by Davenport & Root (1958) and in a simple fashion with application to aerodynamic problems by Liepmann (1952*a*). The result of the theory for the mean-square amplitude of the response is that, if the differential equation for the system is

$$d^2y/dt^2 + \beta\, dy/dt + \omega_0^2 y = F(t), \tag{16}$$

where $F(t)$ is the random forcing function, the mean square of the response is (Liepmann 1952*a*)

$$\overline{y^2} = \int_0^\infty f(\omega)\, d\omega / \{(\omega^2 - \omega_0^2)^2 + \beta^2\omega^2\}, \tag{17}$$

where $f(\omega)$ is the power spectrum of $F(t)$,

$$f(\omega) = (2/\pi) \int_0^\infty \overline{F(t)F(t+\tau)} \cos\omega\tau\, d\tau. \tag{18}$$

If $f(\omega)$ is a slowly varying function compared to the denominator of (17) (small damping, $\beta$), one can write (17) in the approximate form

$$\overline{y^2} = f(\omega_0) \int_0^\infty d\omega / \{(\omega^2 - \omega_0^2)^2 + \beta^2\omega^2\} = \pi f(\omega_0)/2\beta\omega_0^2. \tag{19}$$

Refer to equations (1) and (16) and make the appropriate substitutions from them in (19). The mean square angular deflexion of the disk becomes

$$\overline{\theta^2} = \tfrac{1}{2}\pi \{U f_m(\omega_0)/d\overline{M'^2}\}\, \overline{C_m'^2}/C_{m\theta} C_{m\dot{\theta}}, \tag{20}$$

where the spectral density of the turbulent moment $f_m(\omega_0)$ is evaluated at the natural frequency of disk oscillations.

We have chosen the case of an aluminium disk mounted on a knife edge for our computation of $\overline{\theta^2}$. For this disk the values of the parameters appearing in (20)

are $\omega_0 d/U = 0{\cdot}193$, from figure 6; $Uf_m(\omega_0)/d\overline{M'^2} = 1{\cdot}4$, from figure 12; $\sqrt{\overline{C_m'^2}} = 4{\cdot}7 \times 10^{-3}$, from figure 11; $C_{m\dot{\theta}} = -0{\cdot}05$ if $\omega d/U = 0{\cdot}193$, from figure 10; and $C_{m\theta} = -0{\cdot}108$, from (11) (which is also in agreement with the value of $C_{m\theta}$ computed for free oscillations using (A 11)). Inserting these values in (19) the result is $\sqrt{\overline{\theta^2}} = 0{\cdot}095$. The measured value for this case was $\sqrt{\overline{\theta^2}} = 0{\cdot}122$ (see figure 6). The measured value of $\sqrt{\overline{\theta^2}}$ is 30 % larger than the calculated value. If the static value of $C_{m\theta}$ from figure 5 instead of the dynamic value from (11) or (A 11) is used the measured value of $\sqrt{\overline{\theta^2}}$ is 55 % greater than the calculated value.

We can conclude that the linear representation of (1) for the oscillating disk gives a good qualitative and an approximate quantitative description of the phenomena if one allows for the dependence of $C_{m\theta}$ and $C_{m\dot{\theta}}$ on the dimensionless frequency of oscillation $nd/U$.

## 5. Results and discussion of the cylinder experiments

The experiments on the cylinder were designed to reveal the new features of the unsteady separated flow caused by motion of the separation lines over the longitudinal surface of the cylinder. The cylinder was cut from a large block of Styrofoam plastic. The cylinder length was equal to the diameter, 11·65 in. The cylinder was hollow and fitted with internal supports so that it could be mounted on the moment balance for forced oscillation tests or on ball-bearing pivots for free oscillations tests. The axis of rotation was normal to the axis of symmetry of the cylinder and passed through the centre of the cylinder. Figure 2(*b*), plate 1, is a photograph of the cylinder mounted on the forced-oscillation supports.

### 5.1. *Flow field and static moment*

We made tuft studies of the flow pattern on the surface of the cylinder at Reynolds number $3{\cdot}2 \times 10^5$ in order to locate the regions of separated flow at different angles $\theta$ between the stream direction and the axis of symmetry of the cylinder. The average flow direction indicated by the tufts was used to construct the surface stream line patterns sketched in figure 18. At $\theta = 0$, the flow separates at the edge of the front face and there is a recirculating flow upstream along the longitudinal surface of the cylinder and downstream in the shear layer. At $\theta = 14°$, the flow separates at the front face but partially re-attaches downstream along the windward surface of the cylinder. As $\theta$ increases, the region of attached flow on the windward side grows in size, and the 'separation bubble' ahead of this attached flow region shrinks. The separation bubble disappears at $\theta = 47°$, and the flow is attached everywhere on the windward side of the cylinder.

We used the balance to measure the average moment acting on the cylinder about an axis passing through the centre of the cylinder and normal to the cylinder axis of symmetry and the free stream. The fluctuating-moment signals were averaged with the analogue computer. The results of these measurements are displayed in figure 19. The cylinder is statically stable, $\partial C_m/\partial\theta < 0$, over a rather small range, $-16° < \theta < 16°$. At $\theta = 16°$ the moment attains a minimum value and then begins to increase.

We can understand the reason for the change in the stability if we examine the data of Potter, Shapiro & Murphree (1954), who reported measurements of the pressure distribution on right circular cylinders. The results of their measurements show that the increment in normal force near the upstream end of the cylinder is negative (stabilizing) and is caused by low pressures on the windward

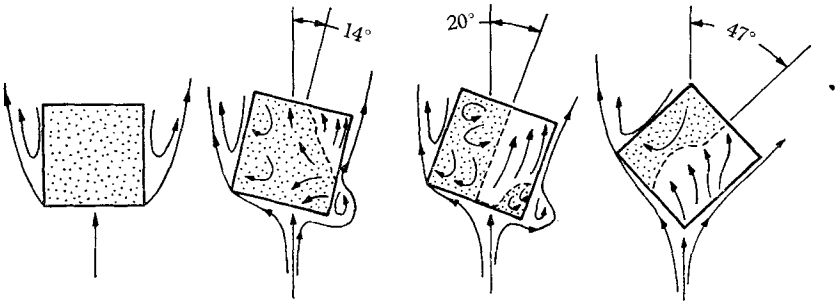


FIGURE 18. The mean-flow direction on the longitudinal surface of the cylinder as revealed by tufts of yarn. $Re = 3{\cdot}2 \times 10^5$, shading indicates separated flow.

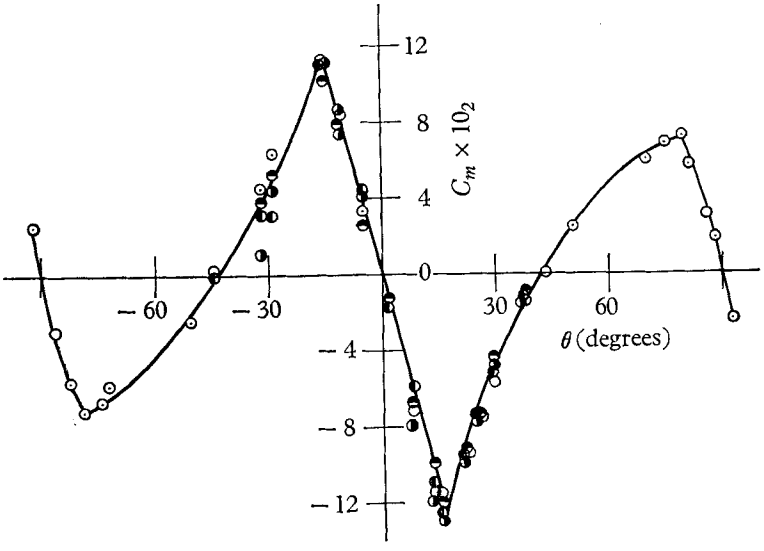


FIGURE 19. Static-moment coefficient of the cylinder $d = l = 11{\cdot}65$ in. Values of $Re \times 10^{-6}$: ◑, 0·126; ⊙, 0·313; ◐, 0·436; ◓, 0·612.

side of the cylinder in the region of the separation bubble. Their pressure-distribution measurements were restricted to the range $-8° < \theta < 8°$, but nevertheless show that the region of negative normal-force increment decreases as $\theta$ increases to $\theta = 8°$. Behind the separation bubble they show that the pressure on the windward surface rises after re-attachment to give a higher pressure on the windward surface than on the leeward surface. This pressure distribution results in a positive normal force that produces a destabilizing moment at stations ahead of the axis of rotation but behind the separation bubble.

Therefore, as $\theta$ increases, and the separation bubble on the windward surface shrinks, the cylinder loses the stabilizing influence of the low pressure in the

separation bubble. The low-pressure region in the separation bubble is replaced by a high-pressure region on the windward side ahead of the pivot and the cylinder becomes statically unstable. As $\theta$ increases, the moment increases and becomes positive reaching a maximum at $\theta \simeq 78°$. The cylinder becomes statically stable again over the range $78° < \theta < 102°$.

The nature of the statically stable region about $\theta = 90°$ was not investigated but it is undoubtedly qualitatively similar to the stable region about $\theta = 0°$.

### 5.2. *Free-oscillation tests*

The cylinder was mounted on ball-bearing pivots allowing free rotation about an axis normal to the stream and the cylinder axis of symmetry passing through the centre of the cylinder. After release from rest with axis of symmetry parallel to the stream, the cylinder oscillated a few times with rapidly increasing amplitude and then began to autorotate at a steady speed. The first few oscillations had amplitudes less than 16 degrees (in the range where the cylinder is statically stable). It was clear, however, that, during the short time that the cylinder oscillated in the statically stable régime, it readily acquired rotational energy from the flow field sufficient to carry it into the statically unstable régime where it began to autorotate.

Repeated observations were made of the first few oscillations after release of the cylinder from rest with $\theta = 0$. The average dimensionless frequency measured with a stop-watch was approximately $nd/U = 0{\cdot}045$. The amplitude of oscillation at the extreme amplitude in each half-cycle rapidly increased but was not very repeatable. It was observed that the cylinder did not always begin divergent oscillations immediately after release from rest but apparently was set in motion by a disturbance in the flow shortly after release from rest. This shows that both the fluctuating turbulent moment acting on the cylinder and the acquisition of rotational energy during oscillation play a part in the divergent motion of the cylinder. Measurements of the fluctuating turbulent moment and the rate of work done on the cylinder during forced oscillations are reported below.

### 5.3. *The buffeting moment produced by turbulence in the wake*

The measurements of the turbulent moment acting on the cylinder were complicated by torsional vibration of the balance and cylinder combination about the moment axis of the balance. The vibration of the cylinder was much more severe than the vibration of the disk and balance combination because the structural and aerodynamic damping of the cylinder were both smaller than the structural and aerodynamic damping of the disk.

We constructed a compensation circuit from analogue computer elements to reduce the spurious signals caused by disk vibration.† The compensation circuit is shown in figure 20. We photographed oscilloscope traces of the vibration signal from the moment balance when the cylinder was displaced and released in still

† We are indebted to E. G. Gilbert for suggesting the method of compensation to us. If we had not used this relatively simple method it would have been necessary to provide mechanical damping or to rebuild a portion of the moment balance.

air. The compensation circuit was adjusted using the frequency 32 c/s and damping determined from the oscilloscope photographs.

The principle of operation of the circuit is relatively simple. If we refer to (15), we may regard $F(t)$ as the moment signal that we desire to measure and $y(t)$ as the output signal of the moment balance which is affected by vibration excitation from $F(t)$ at frequency $\omega_0$. The compensation circuit of figure 20 is arranged to produce electrical signals proportional to the terms $\ddot{y}$, $\beta\dot{y}$, and $\omega_0^2 y$ appearing on the left in (15). The three terms are added together to produce $F(t)$, the desired moment signal, in the summing amplifier labelled 'output' in figure 20.

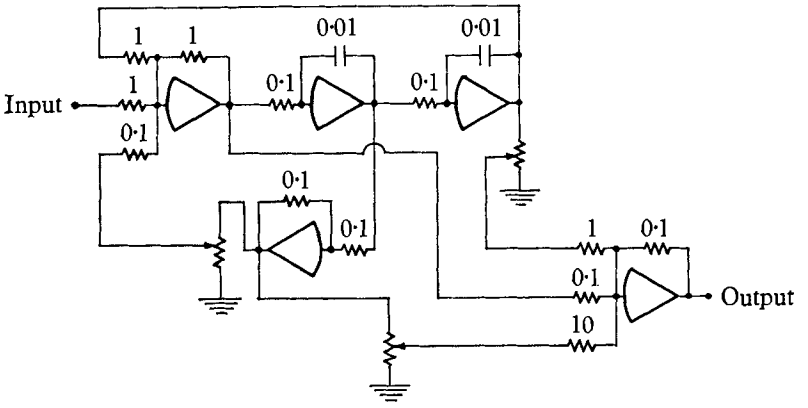


FIGURE 20. Compensation circuit using analogue computer elements to remove the signal caused by vibration of the cylinder-balance combination.

The terms $\dot{y}$ and $\ddot{y}$ for frequencies less than 60 c/s are produced as by-products of the response of a second-order system with higher natural frequency, 159 c/s, and relatively large damping to the signal $y(t)$. This second-order system is represented by the other four amplifiers in figure 20 and gives a relatively noise-free representation of $\dot{y}$ and $\ddot{y}$. The operation of the compensation circuit was checked by vibrating the disk and observing the output on an oscilloscope. To eliminate high-frequency signals, we passed the output signal through a filter with half-power point at 300 c/s.

We used the compensation circuit to determine the root-mean-square turbulent moment and spectrum acting on the cylinder when it was clamped with axis of symmetry parallel to the free stream. The results are shown in figures 11 and 21 in dimensionless form. The root-mean-square moment coefficient is almost twice as large as that measured with the disk. The dimensionless spectra shown in figure 21 are very similar to the disk spectra, figure 12.

The compensation circuit was not adjusted to account for the change in resonance frequency and damping when the cylinder was exposed to the free stream. The flow of air over the cylinder increases the restoring moment and the damping. If adjustment of the compensation circuit to account for these effects had been made at each wind speed, the spectra of figure 21 would have had less scatter. The spectral measurements (figure 21) show that, like the disk, the cylinder moment spectra also scale with the characteristic time $d/U$. The fluctu-

ating moment acting on the cylinder and disk must, therefore, be produced by turbulence in the wake. In fact, the dimensionless spectra of the disk (figure 12) and cylinder moment are almost the same.

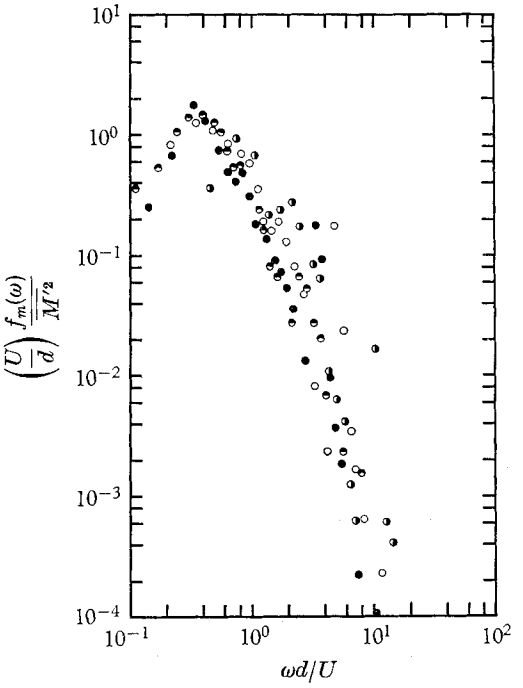


FIGURE 21. Dimensionless power spectra of the fluctuating aerodynamic moment acting on the cylinder with face normal to the flow, $\theta = 0$. Values of $Re \times 10^{-6}$: ◑, 0·137; ○, 0·301; ●, 0·456; ◓, 0·608.

### 5.4. *Rate of work done on the fluid during forced oscillations*

We measured the rate at which work was done on the air by the cylinder during forced oscillations. In these tests the compensation circuit and filter were used to remove partially the vibration signal caused by the cylinder and balance vibration. The methods used to measure the work rate and reduce the data were the same as the methods used in the disk measurements. The results displayed in figure 22 show that $C_{m\dot{\theta}} > 0$ if $nd/U < 0{\cdot}1$ and $C_{m\dot{\theta}} < 0$ if $nd/U > 0{\cdot}1$. This means that free oscillations of the cylinder should be divergent if $nd/U < 0{\cdot}1$, and regular oscillations should be observed for $nd/U > 0{\cdot}1$.

### 5.5. *Regular and divergent oscillations of the cylinder*

We made a very fragile 8 in. diameter cylinder model with a balsa-wood framework covered with Japanese tissue paper in order to obtain low $I^*$ and increase $nd/U$ in the hope that we could observe regular oscillations. Unfortunately, the moment of inertia of the model was so low that it was easily turned about its pivot by the turbulent moment to an angle between the stream and the axis of symmetry greater than 16°. The model immediately began to autorotate. On occasion

the model stopped rotating at a statically stable position, but immediately began rotating again.

We then returned to the original Styrofoam-cylinder model and fastened a long rubber band to the centre of the rear face of the cylinder to provide additional restoring moment and to increase $nd/U$. When the flow was started and the rubber band stretched rather tightly, regular oscillations with random phase and amplitude ($-16° < \theta < 16°$) were observed. If tension in the rubber band was reduced, the amplitude of oscillation soon exceeded 16°, and steady limit-cycle oscillation was observed with little trace of amplitude variation.

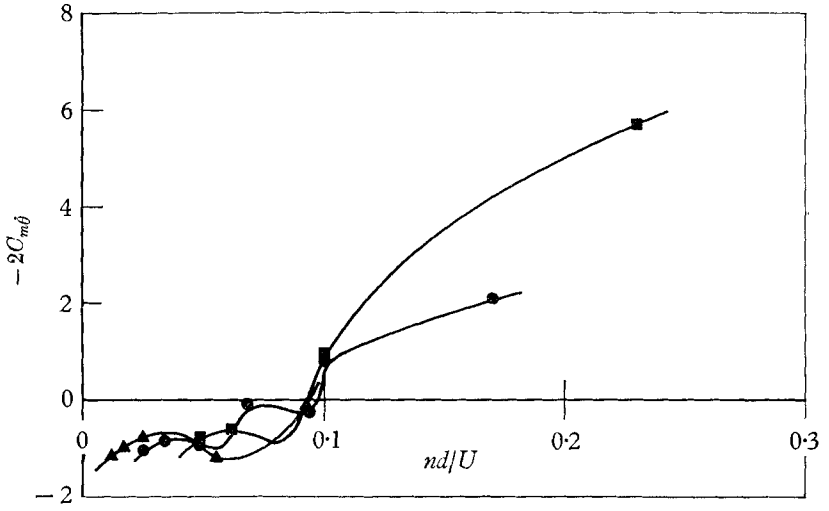


FIGURE 22. Measurements of the derivative of the damping-moment coefficient $C_{m\dot{\theta}}$ during forced oscillations of the cylinder, $\theta_0 = 0{\cdot}24$ rad. Values of $n$ (c/s): ▲, 1·24; ●, 2·53; ■, 4·83.

We can explain the divergent oscillations of a cylinder released from rest in the statically stable régime $-16° < \theta < 16°$ as follows:

After release from rest, with $\theta = 0$, the cylinder is initially set into motion by wake turbulence. If it oscillates at a frequency $nd/U < 0{\cdot}1$, as given by (A 11), the cylinder gains energy because in this range of frequency the motion is not damped, $C_{m\dot{\theta}} > 0$. As soon as the oscillation amplitude exceeds $\theta = \pm 16°$, the cylinder is statically unstable and the cylinder autorotates.

The authors are indebted to Mr Otto Walchner, who introduced us to this problem. We would like to thank Professors E. G. Gilbert, E. O. Gilbert, and R. M. Howe for their helpful advice concerning the use of the analogue computer. We are also grateful for many valuable discussions with Mr Otto Walchner and Professors A. M. Kuethe, W. L. Root and A. F. Messiter and Mr B. J. Tu.

This work has been done under the auspices of the Aeronautical Research Laboratories, Office of Aerospace Research, United States Air Force.

## Appendix

Consider a rigid disk or circular cylinder free to rotate about a fixed diametrical axis passing through the centre of mass of the body. If the angle between the free-stream direction and the normal to the upstream face of the disk or circular cylinder is $\theta$, the equation of motion is

$$I\,d^2\theta/dt^2 = M(t). \tag{A 1}$$

Here $t$ is the time, $M(t)$ is the torque acting on the body defined positive in the same sense as the angle $\theta$, and $I$ is the moment of inertia about the centre of mass. The moment is approximated by the linearized expression

$$M(t) = (\partial M/\partial\theta)_{\theta=0}\theta + (\partial M/\partial\dot{\theta})_{\dot{\theta}=0}\dot{\theta}(t) + M'(t), \tag{A 2}$$

where $\dot{\theta}$ is the time derivative of $\theta$. This approximation implies that the motion of the body introduces only small changes in the moment and that the turbulent moment $M'(t)$ is not appreciably affected by changes in the orientation or motion of the body.

Combining the above equations we obtain

$$I\,d^2\theta/dt^2 - (\partial M/\partial\dot{\theta})_{\dot{\theta}=0}\,d\theta/dt - (\partial M/\partial\theta)_{\theta=0}\theta = M'(t). \tag{A 3}$$

The dimensionless time $t' = tU/d$ is introduced and the whole equation is divided by $qSd$ to obtain

$$I_1^*\,d^2\theta/dt'^2 - C_{m\dot{\theta}}\,d\theta/dt' - C_{m\theta}\theta = C'_m(t'). \tag{A 4}$$

Here

$$I_1^* = (8/\pi)\,I/\rho d^5 = (8/\pi)\,I^*, \tag{A 5}$$

$$C_{m\theta} = \frac{(\partial M/\partial\theta)_{\theta=0}}{qSd}, \tag{A 6}$$

$$C_{m\dot{\theta}} = \frac{(\partial M/\partial\dot{\theta}d/U)_{\dot{\theta}=0}}{qSd}, \tag{A 7}$$

$$C'_m(t') = \frac{M'(t')}{qSd}, \tag{A 8}$$

and $q$ is the dynamic pressure, $S$ is the frontal area $\frac{1}{4}\pi d^2$, $d$ is disk or cylinder diameter, $U$ is free-stream velocity, and $\rho$ is the free-stream density.

In conventional aerodynamic terminology see Etkin (1959) for example,

$$2C_{m\dot{\theta}} = C_{mq} + C_{m\dot{\alpha}}, \tag{A 9}$$

and

$$C_{m\theta} = C_{m\alpha}. \tag{A 10}$$

(A 4) describes a second-order linear system with forcing function $C'_m(t')$ and response $\theta(t')$. The natural frequency of oscillation of the system is

$$\omega d/U = 2\pi n d/U = \sqrt{\{-C_{m\theta}/I_1^* - (C_{m\dot{\theta}}/2I_1^*)^2\}}, \tag{A 11}$$

where $n$ is the frequency, $\omega = 2\pi n$, $C_{m\dot{\theta}}^2 < -4C_{m\theta}I_1^*$, and $C_{m\theta} < 0$.

## REFERENCES

BIRKHOFF, G. & ZARANTONELLO, E. H. 1957 *Jets, Wakes and Cavities*, pp. 115 and 330. New York: Academic Press.

DAVENPORT, W. B. & ROOT, W. L. 1958 *Random Signals and Noise*. New York: McGraw-Hill.

ETKIN, B. 1959 *Dynamics of Flight*. New York: Wiley.

FUNG, Y. C. 1955 *An Introduction to the Theory of Aeroelasticity*. New York: Wiley.

LIEPMANN, H. W. 1952*a* On the application of statistical concepts to the buffeting problem. *J. Aero. Sci.* **19**, 793.

LIEPMANN, H. W. 1952*b* Aspects of the turbulence problem. *J. Appl. Math. Phys.* (*ZAMP*), **3**, 321.

LIN, C. C. 1943 On the motion of a pendulum in a turbulent fluid. *Quart. Appl. Math.* **1**, 1.

POTTER, J. L., SHAPIRO, N. M. & MURPHREE, W. D. 1954 Normal force distributions on right circular cylinders in subsonic flow and supersonic flow. *Ordnance Missile Laboratories, Redstone Arsenal Rep.* no. 2R4F. See also 1954 *J. Aero. Sci.* **22**, 214.

SMITH, A. M. O. 1953 On the motion of a tumbling body. *J. Aero. Sci.* **20**, 73.

WILLMARTH, W. W., HAWK, N. E. & HARVEY, R. L. 1963 Steady and unsteady motions and wakes of freely falling disks. *Phys. Fluids*, **7**, 197.

WILLMARTH, W. W. & HAWK, N. E. 1964 Aerodynamics of the free and forced oscillation of a disk at subsonic speeds. *Office of Aerospace Research U.S. Air Force, ARL Rep.* no. 64-19.